Mechanical properties and structures under the deformation of thiophene copolymers with cyclic siloxane units

Matsumoto, Takuya ; Kashimoto, Masaki ; Kubota, Chihiro ; Horike, Shohei ; Ishida, Kenji ; Mori, Atsunori ; Nishino, Takashi

(Citation)
Polymer Chemistry,13(39):5536-5544

(Issue Date)
2022-10-21

(Resource Type)
journal article

(Version)
Accepted Manuscript

ARTICLE

Mechanical properties and structure under deformation of thiophene copolymers with cyclic siloxane units

Received 00th January 20xx,
Accepted 00th January 20xx

DOI: 10.1039/x0xx00000x

Takuya Matsumoto,*[a] Masaki Kashimoto,[a] Chihiro Kubota,[a] Shohei Horike,[a] Kenji Ishida,[a] Atsunori Mori,[a] and Takashi Nishino*[a]

Polythiophene is a typical semiconductive conjugated polymers; however, thiophene conjugated systems suffer from low flexibility. Although flexible polythiophene with siloxane side chains has been investigated, control of the cross-linking points remains to be achieved. Herein, thiophene copolymers with cyclic siloxane side chains were sthynthesized and the cross-linking points were controled by ring-opening reaction and reduction of tetrathiophene-substituted cyclic siloxane cross-linkers. The obtained thiophene copolymer networks possessed higher glass transition temperatures, larger Young's moduli and strengths, and lower strains at breaking. These behaviors are attributed to the formation of the cross-linking points. In addition, *in situ* X-ray diffraction measurements under cyclic tensile tests comfirmed that the recovery of the crystallite orientation corresponded to the macroscopic deformation of the polythiophene network, better than that of the thiophene copolymer without a network structure.

Introduction

Thiophene rings possess aromaticity because of the π-electron orbitals in their diene structures and lone pairs of chalcogen sulfur atoms. Thus, thiophene rings are promising chemical components of conjugated polymers.[1] In fact, thiophene structures have been introduced into the chemical structures of conjugated polymers through cross-coupling reactions for the fabrication of advanced electronic devices, such as flexible organic photovoltaic cells[2–6], flexible semiconductors[7–11], wearable sensors[8,12–16], and paintable electronic displays[16,17]. As polymer-based electronic devices are prepared through simple painting process, these devices have attractive advantages such as low fabrication cost, low weight, and diversity of form design.[16–20] For the development of these advanced devices, conjugated polymers with high electron conductivities, emission efficiencies, and appropriate mechanical properties, such as flexibility and stretchability, are required.[21–25] In particular, more robust polymer-based electronic devices with high durability against large mechanical deformations are desired in the application of wearable sensors and flexible displays.

Control of the mechanical modulus and elongation at break expands the utility of conjugated polymers. In particular, flexibility and stretchability are achieved in wearable devices that follow the stretching of human skin with a low mechanical modulus, high elongation, and elastic recovery.[8,26,27] However, because conjugated polymers consist of rigid aromatic rings, their fragility is regarded as a challenge. Many researchers have focused on achieving flexibility in conjugated polymers using various approaches. For example, composites of rubber components[15,28–31] and *block* copolymers with flexible segments[32–35] have been suggested. In addition, composites with rubber as the matrix and conductive metallic particles as the fillers were fabricated with drastically increased electronic conductivity by percolation with metallic fillers and formation of electronic conductive pathways. However, the percolation in rubber composites requires loading large amounts of fillers, which decreases flexibility and increases fragility.[36] In addition, large deformations with large strains disconnect the conductive pathways owing to the increased distances between the fillers in the composites. In contrast, conductive elastomers based on *block* copolymers possess microphase-separated structures, such as bi-continuous structures, with the conductive segments self-assembled and distributed homogeneously on the nano scale. Therefore, their high electron conductivities were maintained, even under mechanical deformation. However, stepwise living polymerization techniques are required for the synthesis of thiophene-based *block* copolymers.

Although polythiophenes have garnered significant attention as semiconductive materials for hole transport, polythiophenes without side chains lack solubility in conventional organic solvents, and processability in painting and heat-melting methods.[1,37] Therefore, the substitution of alkyl side chains into thiophene rings has been prompted to improve their solubility in organic solvents and processability and to achieve higher electronic conductivities through self-assembly and crystallization involving side chains.[38–40] Thus, we focused on the effects of polythiophene side chains and introduced flexible dimethylsiloxane groups[19,21,22,41–45] into the side chains of polythiophene in this study. Previously, our group

[a] *Department of Chemical Science and Engineering, Graduate School of Engineering, Kobe University, Rokko, Nada, Kobe, 657-8501, Japan.*

Electronic Supplementary Information (ESI) available: [details of any supplementary information available should be included here]. See DOI: 10.1039/x0xx00000x

reported the flexible properties of polythiophenes with disiloxane side chains.[43–47]

Herein, we focus on random copolymers with 3-dodecylthiophene (3DDT) and thiophenes, including cyclic siloxane as flexible side chains (3CSiT or 3tetraCSiT), as shown in Scheme 1. In the designed thiophene copolymers with even low molar fractions of cyclic siloxane units, we aimed to improve the flexible mechanical properties effectively by utilizing side chains. The cyclic siloxane groups opened and reacted with other siloxane groups under acidic conditions. In addition, thiophene copolymers with tetra-substituted cyclic siloxanes were fabricated. The ring-opening reaction and tetra-substituted monomers can achieve the selective formation of cross-links and control of mechanical properties, including elasticity.

Experimental

Materials.

All chemicals employed for the synthesis and measurements were used as received without further purification. Deionized water was obtained using an Elix Essential UV3 (Merck Millipore Co., Ltd.). Thiophene monomers with cyclic siloxane (3CSiT) and precursor 2-chloro-3-(3-buten-1-yl)-thiophene were prepared using previously reported methods.[47] Poly(3-dodecylthiophene) (P3DDT) was synthesized using [1,3-bis (2,6-diisopropylphenyl) imidazole-2-ylidene] triphenylphosphine nickel(II) dichloride ($NiCl_2(IPr)PPh_3$) following reported methods.[46–48] The number average (M_n) and weight average (M_w) molecular weights of P3DDT were 74,300 and 110,000, respectively. The distribution degree (M_w/M_n) was 1.48.

Characterization methods.

^1H (400 MHz) and ^{13}C (100 MHz) nuclear magnetic resonance (NMR) spectra of the monomer were recorded using a JEOL ECZ400 spectrometer in $CDCl_3$ solution. ^1H (400 MHz) and ^{13}C (100 MHz) NMR spectra of polymers were recorded in $C_2D_2Cl_4$ solution at 70 °C. ^{29}Si (80 MHz) NMR spectrum was recorded in CD_2Cl_2 solution at 25°C. The chemical shifts were expressed in ppm, following $CHCl_3$ (7.26 ppm for ^1H), $C_2D_2Cl_4$ (5.97 ppm for ^1H), $CDCl_3$ (77.2 ppm for ^{13}C), and $C_2D_2Cl_4$ (74.1 ppm for ^{13}C) as the internal standards, and tetramethyl silane (0 ppm for ^{29}Si) as the external standard. Gel permeation chromatography analyses were performed on a high-performance liquid chromatography system (CBM-20A, Shimadzu Co.) equipped with a UV detector at 40 °C using $CHCl_3$ as the eluent with columns (HXR-H and TSK-gel GMHHR-M, TOSOH Co., Ltd.). The molecular weights and polymer distributions were evaluated based on the calibration curve obtained using standard polystyrenes. High-resolution mass spectra (HRMS) were measured with a JEOL JMS-T100LP AccuTOF LC-Plus (ESI) with a JEOL MS-5414DART attachment.

Synthesis of thiophene copolymer with cyclic siloxane (P(3DDT-3CSiT)).

P(3DDT-3CSiT) was synthesized using a method similar to that used for P3DDT synthesis.[47] Into 100 mL tetrahydrofuran (THF), 4.2 g 3DDT (15 mmol) and 0.34 g 3CSiT (0.76 mmol) were dissolved under a nitrogen atmosphere. After adding 1.0 M THF/toluene solution of 2,2,6,6,-tetramethylpiperidinylmagnesium chloride lithium chloride complex solution (TMPMgCl·LiCl; 19 mL, 19 mmol) into the mixture, the solution was stirred at 60 °C for 1 h. Subsequently, 3.2 mL THF solution with 18 mg $NiCl_2(IPr)PPh_3$ (24 μmol) was added, and the solution was stirred at room temperature for 24 h. The reaction was quenched by adding 1 M aqueous HCl and methanol. After filtration, the precipitated solids were purified by Soxhlet elution using acetone to elute the unreacted monomers and oligomers. P(3DDT-3CSiT) was obtained with a yield of 87% (3.9 g).

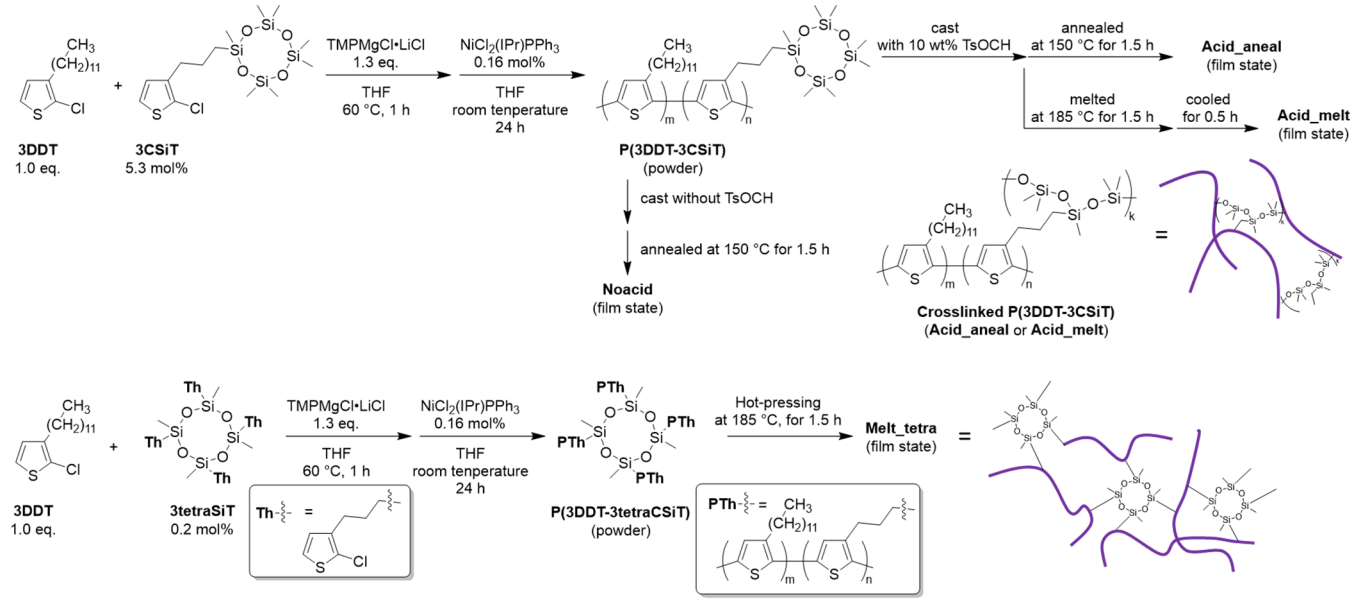

Scheme 1. Syntheses of thiophene copolymers and their cross-linking reaction.

M_n, M_w, and M_w/M_n were 222,000, 312,000, and 1.40, respectively. ^{1}H NMR (400 MHz, $C_2D_2Cl_4$, δ/ppm): 0.07–0.16 (br, 0.9H, –Si–C<u>H</u>$_3$), 0.66–0.78 (t, 0.1H, –CH$_2$–CH$_2$–C<u>H</u>$_2$-Si–), 0.80–0.98 (t, 3.0H, –CH$_2$–CH$_2$–(CH$_2$)$_9$–C<u>H</u>$_3$), 1.18–1.53 (br, 18H, –CH$_2$–CH$_2$–(C<u>H</u>$_2$)$_9$–CH$_3$), 1.62–1.84 (br, 2.0H, –CH$_2$–C<u>H</u>$_2$–(CH$_2$)$_9$–CH$_3$, –CH$_2$–C<u>H</u>$_2$–CH$_2$–Si–), 2.72–2.92 (br, 2.0H, –C<u>H</u>$_2$–CH$_2$–(CH$_2$)$_9$–CH$_3$, –C<u>H</u>$_2$–CH$_2$–CH$_2$–Si–), 6.95–7.05 (br, 1.0H, S–C–C<u>H</u>). ^{13}C NMR (100 MHz, $C_2D_2Cl_4$, δ/ppm): -0.5, 0.9, 1.0, 14.2, 22.8, 27.9, 29.4, 29.6, 29.7, 29.8, 29.8, 30.6, 32.0, 35.7, 128.8, 130.7, 134.0, 140.2

Synthesis of tetrathiophene monomer with cyclic siloxane (3tetraCSiT).

Into 10 mL xylene, 3.0 g 2-chloro-3-(3-buten-1-yl)-thiophene (19 mmol) and 1.1 g 2,4,6,8-tetramethylcyclotetrasiloxane (4.5 mmol) were dissolved. After 79 µm platinum(0)-1,3-divinyl-1,1,3,3-tetramethyldisiloxane complex solution in xylene was added, the mixture was stirred at 60 °C for 23 h. The solution was cooled to room temperature, and the crude product was purified using a silica gel column with hexane as the eluent solvent. The obtained yield of 3tetraCSiT was 55% (2.2 g). ^{1}H NMR (400 MHz, $CDCl_3$, δ/ppm): -0.02–0.12 (br, 12H, C<u>H</u>$_3$ in cyclic siloxane), 0.48–0.64 (m, 8H, –Si–C<u>H</u>$_2$–CH$_2$–CH$_2$–thienyl), 1.52–1.71 (br, 8H, –Si–CH$_2$–C<u>H</u>$_2$–CH$_2$–thienyl), 2.48–2.63 (br, 8H, –Si–CH$_2$–CH$_2$–C<u>H</u>$_2$–thienyl), 6.70–6.81(br, 4H, proton of thiophene ring), 6.95–7.05 (br, 4H, proton of thiophene ring). ^{13}C NMR (100 MHz, $CDCl_3$, δ/ppm): -0.9, -0.6, 1.0, 16.6, 16.9, 23.2, 23.3, 31.2, 122.1, 124.7, 128.0, 138.9. ^{29}Si NMR (80 MHz, $C_2D_2Cl_4$, δ/ppm): -16.8, -18.1, 19.4, 31.2, -32.2, -34.5, 35.3. HRMS (DART–ESI$^+$) *m/z*: calcd for $C_{25}H_{39}Cl_2O_5S_3Si_4$, 699.038; found, 699.104, calcd for $C_{25}H_{39}Cl_3O_5S_3Si_4$, 734.007; found, 734.090.

Synthesis of thiophene copolymer with cyclic siloxane (P(3DDT-3tetraCSiT)).

P(3DDT-3tetraCSiT) was synthesized following the method for P(3DDT-3CSiT).[47] Into 72 mL THF, 3.6 g 3DDT (13 mmol) and 28 mg 3tetraCSiT (31 µmol) were dissolved under a nitrogen atmosphere. After adding 1.0 M THF/toluene solution of TMPMgCl·LiCl (17 mL, 17 mmol) into the mixture, the solution was stirred at 60 °C for 1 h. Subsequently, 5 mL THF solution with 17 mg $NiCl_2$(IPr)PPh_3 (22 µmol) was added, and the solution was stirred at room temperature for 24 h. The reaction was quenched by adding 1 M aqueous HCl and methanol. After filtration, the precipitated solids were purified by Soxhlet elution using acetone to elute the unreacted monomers and oligomers. P(3DDT-3tetraCSiT) was obtained with a yield of 65% (2.4 g). M_n, M_w, and M_w/M_n were 248,000, 369,000, and 1.49, respectively. ^{1}H NMR (400 MHz, $CDCl_3$, δ/ppm): -0.05–0.12 (br, 0.02H, C<u>H</u>$_3$ in cyclic siloxane), 0.68–0.77 (br, 0.01H, –Si–C<u>H</u>$_2$–CH$_2$–CH$_2$–thienyl), 0.80–0.98 (br, 3H, –CH$_2$–CH$_2$–(CH$_2$)$_9$–C<u>H</u>$_3$), 1.15–1.52 (br, 18H, –CH$_2$–CH$_2$–(C<u>H</u>$_2$)$_9$–CH$_3$), 1.62–1.80 (br, 2.0H, –CH$_2$–C<u>H</u>$_2$–(CH$_2$)$_9$–CH$_3$), 2.72–2.92 (br, 2.0H, –C<u>H</u>$_2$–CH$_2$–(CH$_2$)$_9$–CH$_3$), 6.90–7.10 (br, 1.0H, S–C–C<u>H</u>). ^{13}C NMR (100 MHz, $CDCl_3$, δ/ppm): 14.2, 22.8, 29.4, 29.6, 29.7, 29.8, 29.8, 30.6, 32.0, 128.8, 130.7, 134.0, 140.2.

Film preparation and formation of the cross-links of P(3DDT-3CSiT).

Firstly, a 2 wt% $CHCl_3$ solution of P(3DDT-3CSiT) was prepared by dissolving 150 mg P(3DDT-3CSiT) and 15 mg cyclohexyl *p*-toluene sulfonate (TsOCH) as the thermal acid generator[49]. After casting the solution and drying overnight to remove the solvent, cast films with a thickness of approximately 100 µm were prepared. The obtained films were annealed at 150 °C for 1.5 h, and labelled as Acid_anneal. The films were also melted at 185 °C for 1.5 h, slowly cooled for 0.5 h, and labelled as Acid_melt. For comparison, P(3DDT-3CSiT) films without a thermal acid generator were prepared, and labelled as Noacid. P3DDT without a thermal acid generator was fabricated through casting and annealing at 150 °C for 1.5 h.

Preparation of Melt_tetra films.

After melting 150 mg P(3DDT-3tetraCSiT) and pressing at 185 °C, the film was obtained after slow cooling and labelled as Melt_tetra. The thickness of the obtained films was approximately 200 µm.

Measurement of thermal properties.

The thermal decomposition of P(3DDT-3CSiT) and P(3DDT-3tetraCSiT) was measured using a Thermo plus EVOII TG8121 (RIGAKU Co. Ltd.) under a nitrogen atmosphere, using an Al pan. The flow rate was set to 250 mL/min, the heating rate was set to 5 °C/min and the scanning temperature ranged from 150 °C to 500 °C. The temperature corresponding to 5% thermal weight loss (T_{d5}) was defined as the thermal decomposition temperature. Differential scanning calorimetry (DSC) of P3DDT, P(3DDT-3CSiT), and P(3DDT-3tetraCSiT) was performed using a Rigaku DSC8230 instrument under a nitrogen atmosphere using an Al pan. The heating and cooling rates were both 10 °C/min. In the DCS measurements, the heating and cooling processes were performed twice. The second cycle was employed to obtain the DSC curves of the synthesized polythiophenes. The melting temperature (T_m) was defined as the temperature at the top of the endothermic peak during heating.

Measurement of the solubility of the cross-linked P(3DDT-3CSiT) and P(3DDT-3tetraCSiT).

Into 15 g chloroform, 10 mg prepared films were immersed for 17 h. The eluted solutions were evaluated using a UV—vis absorption spectrometer (V-750, JASCO Co., Ltd.). The scan rate of the wavelength was 200 nm/min, the scan range of the wavelength was from 200–900 nm, and the length of the light path was 10 mm. As the Noacid film was completely dissolved in chloroform, the absorbance of diluted solution A was measured, and the molar absorbance coefficient of P(3DDT-3CSiT) ε_{max} was calculated from the Lambert-Beer equation (Equation (1)):

$$A = \varepsilon_{max}\, c\, l \qquad (1)$$

where c is the concentration of the chloroform solution and l is the length of light path, which is equal to 10 mm. From ε_{max}, the concentrations of the eluted solution and weight fractions of the eluted polymers, namely Acid_anneal, Acid_melt, and Melt_tetra, were calculated.

X-ray diffraction measurements.

The X-ray diffraction measurements of the prepared Noacid, Acid_anneal, Acid_melt, and Melt_tetra films were performed using an X-ray diffractometer SmartLab 3 kW (RIGAKU Co. Ltd.) using the θ/2θ method. The X-ray beam was generated at 40 kV and 30 mA with a wavelength of 1.5418 Å (CuKα). The scanning rate was 50°/min, the step size was 0.01°, and the 2θ scanning range was from 2° to 30°. A HyPix-3000 (RIGAKU Co., Ltd.) was employed as the X-ray semiconductor detector.

Dynamic mechanical analysis (DMA).

The DMA measurements were performed using a DVA-20, Itk Co. in the tensile mode. The samples were trimmed into rectangles with dimensions of 30 mm × 5 mm. The initial length, heating speed, mechanical frequency, and maximum loaded strain were 20 mm, 6°/min, 4 Hz, and 0.1%, respectively. The scanning temperature range was from -50 °C to 150 °C. DMA measurements of more than five specimens were performed for each sample, and the obtained mechanical properties were averaged. The glass temperature (T_g) was defined as the temperature at the maximum mechanical loss tanδ.

Mechanical tests.

The tensile tests were performed using an AUTOGRAPH AG-X plus, Shimadzu Co. Ltd. The samples were trimmed into rectangles with the dimensions of 30 × 5 mm. The initial length was 10 mm, and the tensile speed was 10 mm/min. Tensile tests of more than five specimens were performed for each sample, and the obtained mechanical properties were averaged. For the mechanical cyclic tests, the loading and unloading processes were repeated with the maximum strain gradually increasing.

Two-dimentional (2D) X-ray diffraction *in situ* measurements under mechanical cycle tests.

The 2D X-ray diffraction patterns were measured using synchrotron radiation at BL03XU of SPring-8[50] under mechanical cycle tests of Noacid, Acid_anneal, and Melt_tetra. The X-ray wavelength, exposure time, and camera distance were 1.0 Å, 0.8 s, and 0.35 m, respectively. The detector was a Pilatus 2M. A tensile machine (No.10073 LinKAM Scientific Instruments Co. Ltd.) was used for the mechanical cycle tests. The samples were trimmed into rectangles with dimensions of 25 mm × 5 mm, and the crosshead speed was 167 μm/s. The orientation factor *f* under the loading and unloading tensile stress in the cycle tests was calculated from Equation (2) and (3) of the Herman orientation function:

$$\boldsymbol{f} = \frac{3<cos^2\emptyset>-1}{2} \quad (2)$$

$$< \boldsymbol{cos^2\emptyset} >= \frac{\int I sin\emptyset cos^2\emptyset \, d\emptyset}{\int I sin\emptyset \, d\emptyset} \quad (3)$$

where I is the intensity of diffraction, and ϕ is the orientation degree.

Results and discussion

The monomers of P(3DDT-3CSiT) and P(3DDT-3tetraCSiT) were synthesized using methods similar to those used in previous reports.[44,47] In their ^{1}H NMR spectra, the peaks of the methyl groups of the cyclic siloxane moieties were observed at approximately 0 ppm. The copolymerization of their monomers with cyclic siloxanes and 3-DDT was performed using nickel catalyst $NiCl_2(PPh_3)IPr$, as shown in Scheme 1. The polymerizations progressed without by-products. P(3DDT-3CSiT) possessed large solubility into chloroform. In contrast, the solubility of P(3DDT-3tetraCSiT) into chloroform was decreased at room temperature, but P(3DDT-3tetraCSiT) dissolved into chloroform at a temperature higher than 50 °C, and once P(3DDT-3tetraCSiT) had dissolved into chloroform, P(3DDT-3tetraCSiT) in chloroform remained in the solution state even at room temperature. M_w were 312,000 and 369,000 for the obtained copolymers P(3DDT-3CSiT) and P(3DDT-3tetraCSiT) , respectively. These molecular weights were sufficient for the preparation of self-standing films and the investigation of their mechanical properties. The molar fraction of the 3CSiT units in P(3DDT-3CSiT) was 4.2% in the ^{1}H NMR spectrum. Polymerization with a larger molar fraction of 3CSiT progressed insufficiently. In contrast, the peak of the cyclic siloxane units of P(3DDT-3tetraCSiT) was observed slightly. The molar fraction of the cross-linked units in P(3DDT-3tetraCSiT) was 0.2% in the ^{1}H NMR spectrum. The reason would be that the steric hinderance of 3tetraCSiT suppressed its reactivity in copolymerization with 3DDT. This result means that P(3DDT-3tetraCSiT) possessed the network structure involving tetra-armed cross-linking points.

As shown in Figures S11 and S12 in the Supplementary Information, T_{d5} of P(3DDT-3CSiT) and P(3DDT-3tetraCSiT) were observed at 381 °C and 377 °C, respectively. T_{d5} of P3DDT was observed at 370 °C, which indicates that the thermal resistances of P(3DDT-3CSiT) and P(3DDT-3tetraCSiT) were comparable to that of P3DDT, regardless of the cyclic siloxane moieties. In the DSC curves, the melting and crystallization behaviors of P(3DDT-3CSiT) and P(3DDT-3tetraCSiT) were similar to those of P3DDT because the synthesized copolymers contained large fractions of 3DDT units. As shown in Figures S13–S15 in the Supplementary Information, T_m were 155 °C and 160 °C for P(3DDT-3CSiT) and P(3DDT-3tetraCSiT), respectively, and 164 °C for P3DDT.[51] In addition, the crystallization exotherms of P(3DDT-3CSiT) and P(3DDT-3tetraCSiT) appeared at 119 °C and 127 °C, respectively, whereas that of P3DDT was appeared at 131 °C. The melting and crystallization of both the copolymers occurred at slightly lower temperatures than those of P3DDT. The reason for the difference would be that the crystallites of P(3DDT-3CSiT) and P(3DDT-3tetraCSiT) contained cyclic siloxane side chains or their cross-linking points as defects.

The self-standing films of P(3DDT-3CSiT) were prepared by forming cross-links. The P(3DDT-3CSiT) films, including the acid generator TsOCH[49], were prepared using the casting method. The

Table 1. Prepared cross-linked polythiophene films and their thermal and mechanical parameters.

Sample name	Components	Condition	M_w[a]	T_{d5}[b]	T_m[c]	T_g[d]	Young's modulus	Mechanical strength	Elongation at break
				°C	°C	°C	MPa	MPa	%
Noacid	P(3DDT-3CSiT)	Cast and annealed at 150 °C for 1.5 h	312k	381	155	1.0	39 ± 2	9.4 ± 1.2	313 ± 47
Acid_anneal	P(3DDT-3CSiT) 10wt% TsOCH	Cast and annealed at 150 °C for 1.5 h	312k	381	155	5.5	46 ± 3	12.0 ± 1.5	74 ± 23
Acid_melt	P(3DDT-3CSiT) 10wt% TsOCH	Cast, melted at 185 °C for 1.5 h and cooled for 0.5 h	312k	381	155	3.0	41 ± 4	8.1± 1.5	64 ± 7
Melt_tetra	P(3DDT-3tetraCSiT)	Hot-pressed at 185 °C for 1.5 h	369k	377	160	3.8	43 ± 4	8.9 ± 1.1	104 ± 12

[a] Calculated from GPC charts of polythiophenes before cross-liked reaction.

[b] Measured with TGA of polythiophenes before cross-liked reaction.

[c] Measured with DSC of polythiophenes before cross-liked reaction.

[d] Measured with DMA of polythiophenes after cross-liked reaction.

heat treatment decomposed TsOCH and generated acid, which then formed a cross-linker through the ring-opening reaction. Acid_anneal and Acid_melt films were prepared under different thermal heating conditions. On the other hand, the Melt_tetra films inherently possessed cross-linking points without any thermal treatment because the four-armed cross-linker unit 3tetraCSiT was involved in the polymerization process. A Melt_tetra film was also prepared by hot pressing because of the low solubility of P(3DDT-3tetraCSiT) in organic solvents. To compare the structure and mechanical properties, Noacid film without the acid generator and P(3DDT) film without cyclic siloxane side chains were also prepared. The characteristics of the obtained films are summarized in Table 1.

To evaluate the effects of the chemical cross-linking of the P(3DDT-3CSiT) and P(3DDT-3tetraCSiT) films, their solubilities in chloroform were investigated, as shown in Figure 1. The weight fraction ratios of the non-crosslinked components of P(3DDT-3CSiT) and P(3DDT-3tetraCSiT) were calculated from the UV—vis absorption coefficient of the eluted solution after the films were immersed in chloroform for 17 h. Noacid was completely dissolved in chloroform. The UV—vis absorption band was observed at 455 nm, and the molar UV—vis absorption coefficient of P(3DDT-3CSiT) was calculated as $\varepsilon_{max} = 9.3 \times 10^3$ [$cm^{-1}M^{-1}$], as shown in Figure S16 in the Supplementary Information. This absorption band was originated from the π-π* transition of the polythiophene main chains. Based on ε_{max}, the amounts of P(3DDT-3CSiT) and P(3DDT-3tetraCSiT) in the extracted chloroform solutions were evaluated. In the Acid_anneal and Acid_melt films, the weight fractions of the extracted polymers were 3.6 wt% and 0.7 wt%, respectively. This suggests that the Acid_melt film possesses more cross-links through the ring-opening reaction of cyclic siloxane by thermal heating than the Acid_anneal film. During thermal annealing below the melting temperature, the crystallites were sustained and the cross-linking formation by the acid generators progressed in the amorphous region. In contrast, the weight fraction of the extracted polymers of Melt_tetra was 1.5 wt%. The extracted weight fractions of Melt_tetra without cross-linking reactions were comparable to those of the cross-linked P(3DDT-3CSiT) films. This indicates that the tetra-substituted cyclosiloxane comonomers behaved as chemical cross-linking points.

Figure 1. Solubility of Noacid, Acid_anneal, and Melt_tetra.

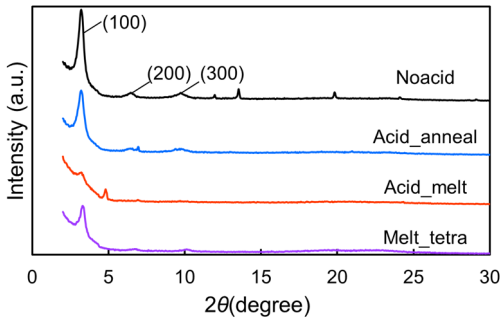

Figure 2. X-ray diffraction profiles of Noacid, Acid_anneal, Acid_melt, and Melt_tetra.

To investigate the crystallinity of the prepared films, X-ray diffraction measurements of Noacid, Acid_anneal, Acid_melt, and Melt_tetra were performed. The X-ray diffraction profiles are shown in Figure 2. For all prepared films, peaks originating from the crystallites of P3DDT were observed at 3.2°, 6.4°, and 9.7°, which were assigned to the (100), (200), and (300) planes, respectively, corresponding to the intermolecular distance in the direction perpendicular to the thiophene rings.[52] Sharp peaks originating from the thermal acid generator TsOCH would be also observed. The diffraction intensities of the (100) plane are as follows: Noacid > Acid_anneal > Acid_melt. The diffraction peaks of Acid_melt almost disappeared, indicating that the cross-linking formation destroyed the crystalline structure and inhibited crystallization.

For Melt_tetra, the films with higher crystallinity provided a lower weight fraction of Melt_tetra extracted into chloroform, compared to Noacid. This higher crystallinity decreased the solubility of chloroform. Diffraction peaks corresponding to the (100), (200), and (300) planes of Melt_tetra was observed at 3.4°, 6.7°, and 10.1°, respectively. This indicates that the intermolecular distance between the polythiophene chains of Melt_tetra through their side chains was lower than that of P(3DDT-3CSiT). This was attributed to the combination of the cyclic siloxane group of the P(3DDT-3CSiT) side chain with the thiophene main chains and the expansion of the intermolecular distance by the bulky cyclic siloxane moieties; however, because the cyclic siloxane moieties in Melt_tetra were mutually cross-linked with different polythiophene chains, the polymer chains were tightly combined and their intermolecular distance slightly decreased.

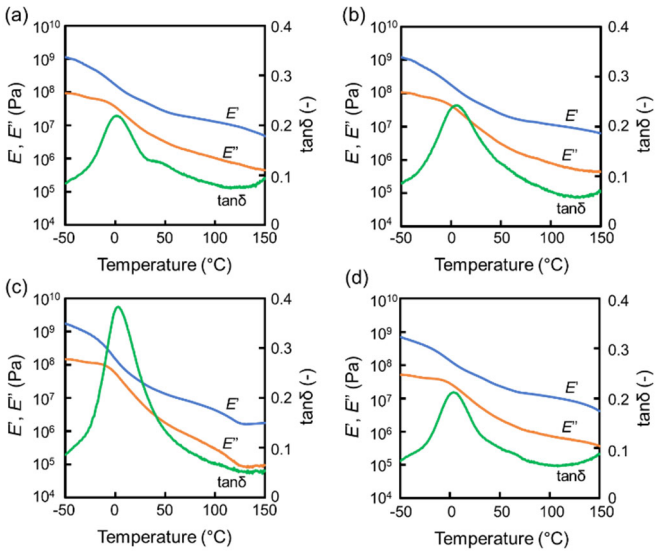

Figure 3. Storage modulus, loss modulus and loss tanδ of (a) Noacid, (b) Acid_anneal, (c) Acid_melt and (d) Melt_tetra.

To investigate on the temperature dependence of the modulus and glass transition temperature of the prepared polythiophene films, DMA measurements were performed from -50 °C to 150 °C. The storage modulus, loss modulus, and mechanical loss tanδ of the films are depicted in Figure 3. The maximum tanδ of the P(3DDT-3CSiT) films was observed at approximately 0 °C, and their storage modulus E'_{25} at 25 °C ranged from 30 MPa to 60 MPa. Therefore, the prepared P(3DDT-3CSiT) films were rubbery-like states at 25 °C. With different fabrication methods, the glass transition temperatures increased from 1.0 °C to 5.5 °C in the following order: Noacid, Acid_anneal, and Acid_melt. The formation of cross-linkers promoted the increase in T_g. The higher T_g of Acid_anneal was attributed to the higher crystallinity of Acid_anneal compared to that of Acid_melt. Acid_melt was cross-linked in the melting state, while the cross-links of Acid_anneal were formed to retain crystallites. Moreover, at temperatures higher than T_g, the storage modulus E' of Acid_melt was lower than those of Noacid and Acid_anneal, as shown in Figure S17 in the Supplementary Information, because Noacid and Acid_anneal possessed higher crystallinity, relative to Acid_melt. Larger plateau regions in E' for Acid_melt, and Acid_anneal with cross-linking were also observed at temperatures higher than 50 °C, compared to the case of Noacid. This result also confirmed that Acid_melt and Acid_anneal possessed cross-linked structures. For Melt_tetra, T_g was 3.8 °C, which is higher than that of Noacid without cross-linkers. In addition, at temperatures higher than 50 °C, the inclination of E' of Melt_tetra decreased, resulting in a plateau-like region of E'. These results indicated that the tetrathiophene-substituted siloxane unit was regarded as a cross-linking point in Melt_tetra in the DMA measurement.

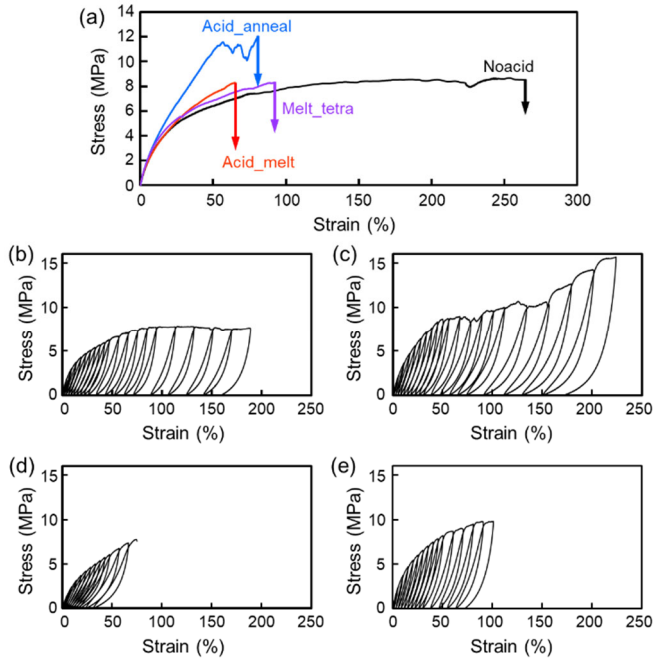

Figure 4. (a) Stress-strain curves of synthesized thiophene copolymers and in cyclic tensile tests of (b) Noacid, (c) Acid_anneal, (d) Acid_melt and (e) Melt_tetra.

The mechanical properties of the prepared polythiophene films were investigated by conducting tensile tests. Their strain-stress curves and mechanical parameters are shown in Figure 4a and Table S1 in the Supplementary Information. Compared with P3DDT without cyclic siloxane moieties, the Young's modulus and tensile strength of

the Noacid film were decreased, whereas its strain at break reached 300%. The Noacid film exhibited a crystallinity similar to that of P3DDT. Therefore, this larger strain at break would be attributed to the flexible cyclic siloxane side chains.[44,45] Moreover, the formation of cross-linkers in the Acid_melt and Acid_anneal films provided larger modulus and lower strain at break than those of the Noacid films. The difference of crystallinity between the Acid_melt and Acid_anneal films caused the slightly larger modulus of the Acid_anneal films than that of the Acid_melt one. The mechanical properties of the Melt_tetra film were similar to those of Acid_anneal and Acid_melt films because of the cross-linker of the tetra-substituted cyclic siloxane in the Melt_tetra film.

Cyclic tensile tests were performed to evaluate the elastic recovery of the cross-linked polythiophenes. All prepared polythiophene films showed plastic deformation and large hysteresis at strains larger than 10%. To compare the cross-linking effect on elastic recovery, the stress-strain curves in the loading and unloading processes with an elongation strain of 50% are shown in Figure S19 in the Supplementary Information. The strain recovery ratios R_{50} were calculated from the strain values before loading and after unloading. The R_{50} values were 80%, 87%, and 91% for the Noacid, Acid_anneal, and Acid_melt films, respectively. The Acid_melt film exhibited the largest elastic recovery ratio because of its cross-link formation and low crystallinity. The Acid_anneal film has a lower crystallinity than the Acid_melt film, which enhanced plastic deformation. In contrast, R_{50} for the Melt_tetra film was 84%, which was higher than that of the Noacid film and lower than those of the Acid_anneal and Acid_melt films. These suggest that the tetra-substituted thiophene formed cross-links in the Melt_tetra films, with a sufficiently low cross-linking degree compared to those of the Acid_anneal and Acid_melt films.

Next, we focused on the effects of cross-linking on the elastic recovery and structural deformation, and performed X-ray diffraction measurements under cyclic tensile deformation using synchrotron radiation. The changes in the crystallite orientation degrees under loading and after unloading were analyzed using the diffraction of the (100) plane as shown in Figure 5. These measurements were performed for the Noacid, Acid_anneal, and Melt_tetra films because their crystallinities were sufficient to evaluate the crystallite orientation under deformation. For the films without stress, the diffraction of the (100) plane were observed as Debye-Scherrer rings, as shown at 0 MPa in Figure 5b. Thus, before the stress was applied, the crystallites were randomly oriented. As the stress was increased, the diffraction ring was gradually changed to arcs in the meridian direction. The changes in the Hermann's orientation degrees of the films are presented in Figure 5c and Figure S20c and S21c in the Supplementary Information. The crystallite orientation of the Noacid film was increased with loading strains larger than 50% and decreased after unloading. However, for strains less than 50%, the orientation degrees gradually increased through repeated loading and unloading. The orientation degrees did not decrease after unloading. These results suggest that when the Noacid film was drawn, the film involved necking and yielding deformation under strains of less than 50%. In addition, after necking was completed, the film was drawn homogenously after elongation with a strain larger than 50%. Therefore, the correlation between the strain and orientation degree of the Noacid film was linear at strains value larger than 50%. The orientation degrees of the Acid_anneal film with high crystallinity and cross-links exhibited the largest repeatability with the loading strains, as shown in Figure 5. For the Melt_tetra film, the orientation degree of the crystallites exhibited higher repeatability when the strain is less than 40%, compared to the Noacid film. However, the orientation degrees at strains larger than 40% strain were dispersed because of the localized deformation under loading strain. These results coincided with the cross-linking degree of tetra-substituted cyclic siloxane moieties.

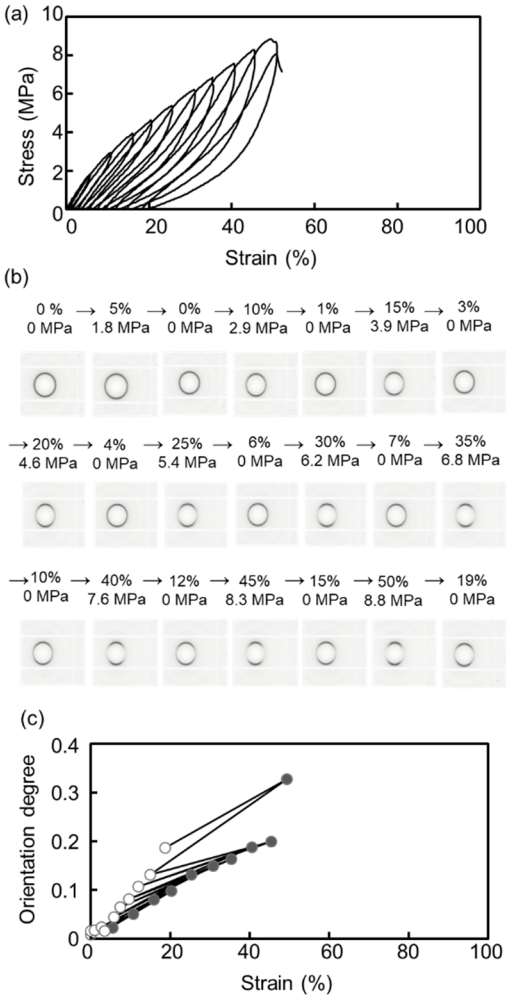

Figure 5. (a) Stress-strain curves, (b) 2D X-ray diffraction images, (c) orientation degrees of Acid_anneal in *in situ* X-ray diffraction pattern measurements under cyclic tensile tests (black circles : loading states, and white circles : unloading states).

Conclusions

In this study, we fabricated thiophene copolymers, P(3DDT-3CSiT) and P(3DDT-3tetraCSiT), including cyclic siloxanes with high molecular weights. Self-standing films were prepared using casting and hot-pressing methods. Through thermal acid treatments involving an acid thermogenerator or

copolymerization with tetra-substituted cyclic siloxane units, cross-linked networks were formed, which provided lower solubility in organic solvents, and increased the glass transition temperature. The Young's modulus and mechanical strength increased, and larger elastic recoveries were observed due to the presence of cross-linking points and crystallization, relative to the thiophene copolymer without a network structure. In addition, *in situ* X-ray diffraction measurements were performed during cyclic tensile testing to investigate the correlation between the strain and crystallite orientation. The recovery of the crystallite orientation was obtained to be the highest for the thiophene copolymer with a network structure after acid treatment. The crystallite orientation decreased for the copolymer containing tetra-substituted cyclic siloxane units without acid treatment, whereas the copolymer without a network structure showed no orientation recovery. Therefore, in this work, we clarified the effects of the network structure of thiophene copolymers with cyclic thiophene groups on their mechanical properties and structural deformation. These results suggested molecular designs for the control of the mechanical properties of π-conjugated polymers such as polythiophenes in advanced electronic devices.

Conflicts of interest

There are no conflicts to declare.

Acknowledgements

The synchrotron radiation experiments were performed at BL03XU of SPring-8 with the approval of the Japan Synchrotron Radiation Research Institute (JASRI) (Proposal No. 2019A7209, 2019B7259, 2020A7208, 2021A7208, 2021B7258, and 2022A7209). The authors would like to acknowledge Prof. Kentaro Okano and Mr. Kengo Inoue (Graduate School of Engineering, Kobe University) for supporting NMR measurements at 70 °C.

Notes and references

1 G. B. Street and T. C. Clarke, *IBM J. Res. Dev.*, 1981, **25**, 51–57.
2 P. W. M. Blom, V. D. Mihailetchi, L. J. A. Koster and D. E. Markov, *Adv. Mater.*, 2007, **19**, 1551–1566.
3 H. Zhou, L. Yang and W. You, *Macromolecules*, 2012, **45**, 607–632.
4 M. Kaltenbrunner, M. S. White, E. D. Głowacki, T. Sekitani, T. Someya, N. S. Sariciftci and S. Bauer, *Nat. Commun.*, 2012, **3**, 770.
5 A. Facchetti, *Mater. Today*, 2013, **16**, 123–132.
6 D. J. Lipomi, B. C. K. Tee, M. Vosgueritchian and Z. Bao, *Adv. Mater.*, 2011, **23**, 1771–1775.
7 A. Rudge, I. Raistrick, S. Gottesfeld and J. P. Ferraris, *Electrochim. Acta*, 1994, **39**, 273–287.
8 T. Someya, T. Sekitani, S. Iba, Y. Kato, H. Kawaguchi and T. Sakurai, *Proc. Natl. Acad. Sci.*, 2004, **101**, 9966–9970.
9 H. Sirringhaus, *Adv. Mater.*, 2014, **26**, 1319–1335.
10 H. Sirringhaus, *Adv. Mater.*, 2005, **17**, 2411–2425.
11 S. R. Forrest, *Nature*, 2004, **428**, 911–918.
12 S. Savagatrup, E. Chan, S. M. Renteria-Garcia, A. D. Printz, A. V Zaretski, T. F. O'Connor, D. Rodriquez, E. Valle and D. J. Lipomi, *Adv. Funct. Mater.*, 2015, **25**, 427–436.
13 C. Pang, C. Lee and K.-Y. Suh, *J. Appl. Polym. Sci.*, 2013, **130**, 1429–1441.
14 W. Gao, H. Ota, D. Kiriya, K. Takei and A. Javey, *Acc. Chem. Res.*, 2019, **52**, 523–533.
15 S. Chen, Y. Wei, X. Yuan, Y. Lin and L. Liu, *J. Mater. Chem. C*, 2016, **4**, 4304–4311.
16 Y. S. Rim, S.-H. Bae, H. Chen, N. De Marco and Y. Yang, *Adv. Mater.*, 2016, **28**, 4415–4440.
17 T. Sekitani, H. Nakajima, H. Maeda, T. Fukushima, T. Aida, K. Hata and T. Someya, *Nat. Mater.*, 2009, **8**, 494–499.
18 J. H. Cho, J. Lee, Y. Xia, B. Kim, Y. He, M. J. Renn, T. P. Lodge and C. Daniel Frisbie, *Nat. Mater.*, 2008, **7**, 900–906.
19 J. Lee, A. R. Han, H. Yu, T. J. Shin, C. Yang and J. H. Oh, *J. Am. Chem. Soc.*, 2013, **135**, 9540–9547.
20 H. Yan, Z. Chen, Y. Zheng, C. Newman, J. R. Quinn, F. Dötz, M. Kastler and A. Facchetti, *Nature*, 2009, **457**, 679–686.
21 Y. Kim, O. Y. Kweon, Y. Won and J. H. Oh, *Macromol. Res.*, 2019, **27**, 625–639.
22 O. Y. Kweon, S. K. Samanta, Y. Won, J. H. Yoo and J. H. Oh, *ACS Appl. Mater. Interfaces*, 2019, **11**, 26134–26143.
23 D. J. Lipomi, M. Vosgueritchian, B. C.-K. Tee, S. L. Hellstrom, J. A. Lee, C. H. Fox and Z. Bao, *Nat. Nanotechnol.*, 2011, **6**, 788–792.
24 S. C. B. Mannsfeld, B. C.-K. Tee, R. M. Stoltenberg, C. V. H.-H. Chen, S. Barman, B. V. O. Muir, A. N. Sokolov, C. Reese and Z. Bao, *Nat. Mater.*, 2010, **9**, 859.
25 Y. Wang, C. Zhu, R. Pfattner, H. Yan, L. Jin, S. Chen, F. Molina-Lopez, F. Lissel, J. Liu, N. I. Rabiah, Z. Chen, J. W. Chung, C. Linder, M. F. Toney, B. Murmann and Z. Bao, *Sci. Adv.*, 2017, **3**, 1–11.
26 S. Wang, J. Xu, W. Wang, G.-J. N. Wang, R. Rastak, F. Molina-Lopez, J. W. Chung, S. Niu, V. R. Feig, J. Lopez, T. Lei, S.-K. Kwon, Y. Kim, A. M. Foudeh, A. Ehrlich, A. Gasperini, Y. Yun, B. Murmann, J. B.-H. Tok and Z. Bao, *Nature*, 2018, **555**, 83–88.
27 M. L. Hammock, A. Chortos, B. C.-K. Tee, J. B.-H. Tok and Z. Bao, *Adv. Mater.*, 2013, **25**, 5997–6038.
28 K.-Y. Chun, Y. Oh, J. Rho, J.-H. Ahn, Y.-J. Kim, H. R. Choi and S. Baik, *Nat. Nanotechnol.*, 2010, **5**, 853–857.
29 M. Park, J. Im, M. Shin, Y. Min, J. Park, H. Cho, S. Park, M.-B. Shim, S. Jeon, D.-Y. Chung, J. Bae, J. Park, U. Jeong and K. Kim, *Nat Nano*, 2012, **7**, 803–809.
30 H. Liu, J. Gao, W. Huang, K. Dai, G. Zheng, C. Liu, C. Shen, X. Yan, J. Guo and Z. Guo, *Nanoscale*, 2016, **8**, 12977–12989.
31 H. Liu, Q. Li, S. Zhang, R. Yin, X. Liu, Y. He, K. Dai, C. Shan, J. Guo, C. Liu, C. Shen, X. Wang, N. Wang, Z. Wang, R. Wei and Z. Guo, *J. Mater. Chem. C*, 2018, **6**, 12121–12141.
32 C.-A. Dai, W.-C. Yen, Y.-H. Lee, C.-C. Ho and W.-F. Su, *J. Am. Chem. Soc.*, 2007, **129**, 11036–11038.
33 E. Lee, B. Hammer, J.-K. Kim, Z. Page, T. Emrick and R. C. Hayward, *J. Am. Chem. Soc.*, 2011, **133**, 10390–10393.

34 Q. Zhang, A. Cirpan, T. P. Russell and T. Emrick, *Macromolecules*, 2009, **42**, 1079–1082.

35 Y.-C. Chiang, S. Kobayashi, T. Isono, C.-C. Shih, T. Shingu, C.-C. Hung, H.-C. Hsieh, S.-H. Tung, T. Satoh and W.-C. Chen, *Polym. Chem.*, 2019, **10**, 5452–5464.

36 R. F. Gibson, *Compos. Struct.*, 2010, **92**, 2793–2810.

37 J. E. Frommer, *Acc. Chem. Res.*, 1986, **19**, 2–9.

38 S. Hotta, S. D. D. V Rughooputh, A. J. Heeger and F. Wudl, *Macromolecules*, 1987, **20**, 212–215.

39 R. L. Elsenbaumer, K. Y. Jen and R. Oboodi, *Synth. Met.*, 1986, **15**, 169–174.

40 I. Osaka and R. D. McCullough, *Acc. Chem. Res.*, 2008, **41**, 1202–1214.

41 J. Lee, A. R. Han, J. Kim, Y. Kim, J. H. Oh and C. Yang, *J. Am. Chem. Soc.*, 2012, **134**, 20713–20721.

42 A. R. Han, J. Lee, H. R. Lee, J. Lee, S. H. Kang, H. Ahn, T. J. Shin, J. H. Oh and C. Yang, *Macromolecules*, 2016, **49**, 3739–3748.

43 J. Shen, I. Sugimoto, T. Matsumoto, S. Horike, Y. Koshiba, K. Ishida, A. Mori and T. Nishino, *Polym. J.*, 2019, **51**, 257–263.

44 J. Shen, K. Fujita, T. Matsumoto, C. Hongo, M. Misaki, K. Ishida, A. Mori and T. Nishino, *Macromol. Chem. Phys.*, 2017, **218**, 1700197.

45 J. Shen, M. Kashimoto, T. Matsumoto, A. Mori and T. Nishino, *Polym. J.*, 2020, **52**, 1273–1278.

46 K. Fujita, Y. Sumino, K. Ide, S. Tamba, K. Shono, J. Shen, T. Nishino, A. Mori and T. Yasuda, *Macromolecules*, 2016, **49**, 1259–1269.

47 C. Kubota, M. Kashimoto, R. Yamashita, K. Okano, M. Horie, M. Funahashi, T. Matsumoto, T. Nishino and A. Mori, *Bull. Chem. Soc. Jpn.*, 2022, **95**, 882–888.

48 S. Tamba, S. Tanaka, Y. Okubo, H. Meguro, S. Okamoto and A. Mori, *Chem. Lett.*, 2011, **40**, 398–399.

49 A. Sudo, H. Yamashita and T. Endo, *J. Polym. Sci. Part A Polym. Chem.*, 2011, **49**, 3631–3636.

50 H. Masunaga, H. Ogawa, T. Takano, S. Sasaki, S. Goto, T. Tanaka, T. Seike, S. Takahashi, K. Takeshita, N. Nariyama, H. Ohashi, T. Ohata, Y. Furukawa, T. Matsushita, Y. Ishizawa, N. Yagi, M. Takata, H. Kitamura, K. Sakurai, K. Tashiro, A. Takahara, Y. Amamiya, K. Horie, M. Takenaka, T. Kanaya, H. Jinnai, H. Okuda, I. Akiba, I. Takahashi, K. Yamamoto, M. Hikosaka, S. Sakurai, Y. Shinohara, A. Okada and Y. Sugihara, *Polym. J.*, 2011, **43**, 471–477.

51 S. L. Liu and T. S. Chung, *Polymer (Guildf).*, 2000, **41**, 2781–2793.

52 K. Tashiro, K. Ono, Y. Minagawa, M. Kobayashi, T. Kawai and K. Yoshino, *J. Polym. Sci. Part B Polym. Phys.*, 1991, **29**, 1223–1233.